NUWC-NPT Technical Report 12,183
1 September 2015

Effects of Weave Styles and Crimp Gradients on Damage Tolerance and Energy-Absorption Capacities of Woven Kevlar/Epoxy Composites

Paul V. Cavallaro
Ranges, Engineering, and Analysis Department

NEWPORT

Naval Undersea Warfare Center Division
Newport, Rhode Island

PREFACE

This research was funded by NUWC Division Newport's Chief Technology Office (Neil J. Dubois (00T1)) and the Office of Naval Research. The principal investigator was Paul V. Cavallaro (Code 7023).

The technical reviewer was Matthew E. Johnson (Code 7023).

The author gratefully acknowledges Martin S. Leff (Code 7014) and Arun Shukla of the University of Rhode Island and his students for their assistance with the experiments. Special thanks are also given to JPS Composite Materials Inc. for providing the Kevlar woven fabrics and technical data and to Core Composites Inc. for fabricating the composite laminates.

Reviewed and Approved: 1 September 2015

Eric S Spigel

Eric S. Spigel
Head, Ranges, Engineering, and Analysis Department

REPORT DOCUMENTATION PAGE

Form Approved
OMB No. 0704-0188

1. REPORT DATE (*DD-MM-YYYY*)	2. REPORT TYPE	3. DATES COVERED (*From – To*)
01-09-2015	Technical Report	

4. TITLE AND SUBTITLE

Effects of Weave Styles and Crimp Gradients on Damage Tolerance and Energy-Absorption Capacities of Woven Kevlar/Epoxy Composites

5a. CONTRACT NUMBER

5b. GRANT NUMBER

5c. PROGRAM ELEMENT NUMBER

6. AUTHOR(S)

Paul V. Cavallaro

5.d PROJECT NUMBER

5e. TASK NUMBER

5f. WORK UNIT NUMBER

7. PERFORMING ORGANIZATION NAME(S) AND ADDRESS(ES)

Naval Undersea Warfare Center Division
1176 Howell Street
Newport, RI 02841-1708

8. PERFORMING ORGANIZATION REPORT NUMBER

TR 12,183

9. SPONSORING/MONITORING AGENCY NAME(S) AND ADDRESS(ES)

Naval Undersea Warfare Center Division
1176 Howell Street
Newport, RI 02841-1708

10. SPONSORING/MONITOR'S ACRONYM

NUWC

11. SPONSORING/MONITORING REPORT NUMBER

12. DISTRIBUTION/AVAILABILITY STATEMENT

Approved for public release; distribution is unlimited.

13. SUPPLEMENTARY NOTES

14. ABSTRACT

This research investigates the effects of weave styles and crimp gradients (CGs) on the damage-tolerance levels and energy-absorption capacities of woven fabric-reinforced polymer (WFRP) composites. A comparative study was conducted to determine the specific failure mechanisms including fiber/matrix cohesive failures, matrix cracking, fiber breakage, and fiber buckling resulting from static and dynamic loading events. The tests included flexure, short beam shear, drop impact, flexure-after-impact, ballistic impact, and split Hopkinson compression bar (SHCB) and were performed on 20-ply Kevlar/epoxy WFRP laminates. Laminates of three different Kevlar fabric weave styles were fabricated using plain, 2x2 twill, and 4H satin weaves. A fourth fabricated laminate used a mixture of weave styles—forming a hybrid CG construction. The experimental results demonstrated (1) that weave style selections and CGs can positively influence the spatial and temporal distributions of stress resulting from severe loading events and (2) that the fiber/matrix cohesive zone stresses that often lead to delaminations can be reduced. Accordingly, the dependence of mechanical performance on weave styles, crimp contents, and CGs can be exploited to increase the damage-tolerance levels and energy-absorption capacities in WFRP composites.

15. SUBJECT TERMS

Crimp Crimp Gradients Energy Absorption Experimental Mechanics Fabrics Finite Element Analysis
Functionally Graded Impact Fracture Kevlar Woven Composites Woven Fabric-Reinforced Polymer Composites

16. SECURITY CLASSIFICATION OF:			17. LIMITATION OF ABSTRACT	18. NUMBER OF PAGES	19a. NAME OF RESPONSIBLE PERSON
a. REPORT	b. ABSTRACT	c. THIS PAGE			Paul V. Cavallaro
Unclassified	Unclassified	Unclassified	SAR	38	19b. TELEPHONE NUMBER (*Include area code*) 401-832-5082

TABLE OF CONTENTS

LIST OF ILLUSTRATIONS

Figure **Page**

LIST OF TABLES

Table **Page**

LIST OF ABBREVIATIONS AND ACRONYMS

2-D	Two-dimensional
3-D	Three-dimensional
AET	Acceptable energy threshold
BEBT	Bernoulli-Euler Beam theory
BVID	Barely visible impact damage
CFRP	Carbon-fiber-reinforced polymer
CG	Crimp gradient
CT	Computer tomography
DIC	Digital image correction
DoE	Design of experiments
FEM	Finite element model
GFRP	Glass-fiber-reinforced polymer
gpd	Grams per denier
ILSS	Interlaminar shear stress
J	Joule
MPa	Megapascal
N	Newton
NDI	Nondestructive inspection
PPS	Polyphenylene sulfide
RCC	Right circular cylinder
SHCB	Split Hopkinson compression bar
SYM	Symmetric laminar stacking sequence with respect to midplane
TPU	Thermoplastic polyurethane
UD	Unidirectional
WFRP	Woven fabric-reinforced polymer

EFFECTS OF WEAVE STYLES AND CRIMP GRADIENTS ON DAMAGE TOLERANCE AND ENERGY-ABSORPTION CAPACITIES OF WOVEN KEVLAR/EPOXY COMPOSITES

1. INTRODUCTION

Woven fabric-reinforced polymer (WFRP) composites are becoming the material of choice for lightweight structures because of their high strength-to-weight ratios, directional tailorability, and strength dependencies on strain rates. These highly engineered materials are increasingly sought after for use in structures and protective devices required to operate and survive against severe dynamic loading events such as blast, ballistic and fragment impacts, and mechanical shock. These composites, however, are not without weaknesses and vulnerabilities. For example, two-dimensional (2-D) WFRP composites are inherently weak against loads applied off-axis to the fibers and are susceptible to unique failure mechanisms including fiber breakage and buckling, matrix shearing and cracking, cohesive failures at the fiber/matrix interfaces, delaminations, and edge effects.

The "weak" directional stresses for a laminated material system include the transverse normal stress σ_{zz}, the interlaminar shear stresses (ILSSs) σ_{zx} and σ_{zy}, and the transverse shear stresses τ_{xz} and τ_{yz} (derivations and discussions of laminate stress components are provided by Jones[1]). These stresses lead to the initiation of damage at the microscale in the form of intra-ply matrix cracks, cohesive failures at the individual fiber/matrix interfaces within the yarns, elongation or buckling of individual fibers, and fiber breakage.

As the loading increases, damage evolves to the mesoscale exhibiting further intra-ply and newly formed inter-ply matrix cracks, matrix shearing, distortion and shearing of yarn cross sections, and cohesive failures in the form of delaminations at the yarn/matrix interfaces. Stiffness reductions begin to appear, and laminate deformations become evident. Further loading leads to increased intra-ply and inter-ply matrix crack growth, crack bridging, yarn buckling and pull-out failures, yarn fractures, global laminate deformations, and eventual first-ply failure followed by multi-ply failures and loss of load-carrying capacities. Additionally, WFRP laminates exhibit lower fracture toughness than do metals and can have greater dependence on mixed-mode fracture behaviors because of the weak directional stresses.

Failure mechanisms in WFRP composites are critically important to the composites community. Experimental and computational studies have been performed to identify failure mechanisms, fracture initiations, and crack-propagation modes in woven composites subject to static and dynamic loading events.[2–13] Computational methods, however, have not evolved to the extent necessary to predict damage initiation and propagation as functions of woven-fabric architectures. This lag can be attributed to the difficulties that often arise from the need to characterize the constitutive behaviors and damage mechanisms across multiple material length scales (for example, fiber, yarn, fabric, laminate, structure).

Because finite element models (FEMs) are often size limited, the fiber-to-structure scales cannot be bridged by direct, three-dimensional (3-D) multicontinuum representations. Despite the FEM size limitation, improving the performance of WFRP composites is not impossible and modifications to the woven architectures can be readily evaluated through experiments.

The research documented in this report had three main objectives: (1) investigate damage mechanisms produced in WFRP composites subjected to both static and severe dynamic loading events, (2) determine the influence of weave styles on energy-absorption levels, and (3) demonstrate that sizable increases in damage tolerance and energy-absorption capacities may be achieved by using crimp gradient architectures.

2. PUBLISHED RESEARCH RELATED TO IMPACT RESPONSE, DAMAGE MECHANISMS, FRACTURE, AND CRIMP

This section briefly describes some of the research studies that explored the impact response behaviors, damage mechanisms, fracture propagations, and crimp effects in WFRP composites and textiles—all of which have ultimately contributed to advancing the science for improving the damage-tolerance levels and energy-absorption capacities of WFRP composites and textiles.

Kim and Sham[2] provided a review of modes I and II interlaminar fracture toughnesses, delamination damage mechanisms, and the low-energy impact response of woven-fabric laminates. Having compared woven and unidirectional (UD) cross-ply laminate behaviors, they found that the rough fabric surfaces and resin-rich interlaminar regions associated with woven laminates contributed to larger plastic yield zones that increased fracture toughness levels. Kim and Sham[2] identified that delaminations often resulted from mixed-mode effects and that low-energy impacts were dominated by mode II shear behavior in bending. Their research also investigated fiber-surface treatments using silane agents to increase fracture toughness.

Ullah et al.[3] performed dynamic flexure testing of 4-ply woven-glass and woven-carbon laminates using a pendulum fixture. Both laminates were constructed of twill (2x2) fabric architectures and thermoplastic polyurethane (TPU) matrices. Computer tomography (CT) scans were used to examine the damage zones, which revealed that the damage mechanisms consisted of matrix cracking, delaminations, yarn debonding, and fiber breakage. Numerical FEM was performed using cohesive zone elements, quadratic stress criterion for damage initiation, and the Benzeggagh-Kenane criterion for damage evolution. The carbon-fiber-reinforced polymer (CFRP) laminates exhibited lower fracture toughness and higher impact strengths than did the glass-fiber-reinforced polymer (GFRP) laminates. The FEM results correlated to the test results and captured the sequence of failure modes.

Ullah et al.[4] performed quasi-static on- and off-fiber axis tension and three-point flexure tests of twill (2x2)-woven carbon laminates reinforced with a TPU matrix. Ullah et al.[4] used digital image correlation (DIC) to measure the in-plane shear properties using ±45° off-axis tension tests. The on-fiber axis tensile tests exhibited quasi-brittle fracture behaviors; the off-fiber axis tensile behavior was significantly nonlinear at the low and high stress levels. Two-dimensional FEM using homogenized plies with orthotropic properties and cohesive zone elements was conducted at the mesoscale to simulate delamination damage resulting from large bending deflections. The experimental and predicted load-versus-bending deflection behaviors achieved good agreement as did their experimental and predicted delamination damage sizes.

Park and Jeng[5] evaluated the impact behaviors of materially hybridized laminates consisting of woven Kevlar-29 and Spectra-900 fibers with a vinylester resin system. Both inter-ply and intra-ply hybrid laminates were tested using a dart impact test machine. Impact loads and damage shapes were compared. The inter-ply hybrid laminates absorbed most of the impact energy through the formation of delaminations, and the intra-ply laminates generally absorbed the impact energy through deformation of the Spectra fibers.

Naik et al.[6] performed 3-D FEM modeling of thin woven and UD cross-ply E-glass/epoxy laminated plates subjected to low-velocity impact. An in-plane failure function based on the Tsai-Hill criterion[1] was used to assess damage initiation during impact (failures occurred when the failure function achieved a magnitude ≥ 1.0). Their results demonstrated that the in-plane failure function magnitudes were (1) greater along the impact surfaces versus the rear surfaces of the woven laminates, suggesting that in-plane failures would initiate near the impact surfaces and (2) greater along the rear surfaces of the UD cross-ply laminates, suggesting that in-plane failures would initiate near the rear surfaces. The failure function magnitudes reported for the cross-ply laminates, however, were approximately five times greater than those of the woven laminates. Based on the in-plane failure criterion alone, the woven laminates achieved a five times greater damage-initiation threshold for low-velocity impact than that for the UD cross-ply laminates.

Thatte et al.[7] performed both drop impact tests and numerical modeling on 10-ply, basket-woven E-glass/epoxy laminates and plain-woven AS4 carbon/epoxy laminates subjected to a range of impact energies. Impact loads and energy absorptions obtained from the models were compared to the experimental results. Results of the glass/epoxy laminate models agreed well with the test data as no significant damage occurred; however, because the models did not include damage criteria, the carbon/epoxy laminate predictions deviated from the test data.

M. Karahan and N. Karahan[8] investigated the effects of yarn crimp on the tensile properties of carbon/epoxy and hybrid carbon-aramid/epoxy laminates constructed with plain and twill weaves. Two plain-woven carbon/epoxy laminate specimens—one with balanced crimp and one with unbalanced crimp—were tested in quasi-static uniaxial tension. Compared to the balanced crimp specimen, the unbalanced crimp specimen exhibited a 20% increase in warp direction tensile strength. Warp direction tensile strength of the twill laminate was approximately 8% greater than that found in the plain-woven laminate with unbalanced crimp. M. Karahan and N. Karahan[8] further concluded that increased crimp reduced laminate strength and stiffness levels.

Naik et al.[9] investigated the impact behaviors and damage-tolerance levels of hybridized plain-woven glass-twill and plain-woven carbon/epoxy laminates subjected to drop impact testing. The laminates were dually hybridized in that hybridization of the fiber materials and hybridization of the plain- and twill-woven architectures were performed. The hybrid laminates exhibited reduced notch sensitivity compared to the all-glass and all-carbon laminates. The duration of impact loading time was longer for the hybrid laminates with the glass layers positioned at the surfaces and the carbon layers positioned as internal (core) layers.

Daggumati et al.[10] examined the damage behaviors of 8-ply satin (5H)-woven carbon/polyphenylene sulfide (PPS) laminates subjected to static tensile tests. They used acoustic emission measurements and microscopic analysis to identify failure initiation thresholds and locations. Under uniaxial tension, the major damage prior to failure was cracking within the weft yarn fiber bundles.

Alemi-Ardakani et al.[11] applied a Taguchi-based design of experiments (DoE) for optimizing the lay-up design process of Twintex (commingled polypropylene and glass fibers) laminates to maximize impact energy absorption capacities. Plies of UD, plain- and twill-woven architectures were evaluated. Their experiments consisted of drop-weight impact and pre- and post-impact four-point bend tests performed on laminated plates constructed of mixed and consistent architectures. The results demonstrated that (1) greater impact energy-absorption capacities were obtained for laminates constructed with mixed architectures and having woven layers positioned near the surfaces and (2) the consistent woven laminates retained the majority of pre-impact flexure modulus compared to that retained by the consistent UD laminates.

Research by Cavallaro and Sadegh[14] was performed on single-ply woven fabrics subjected to ballistic impact using ABAQUS/Explicit.[15] Their numerical modeling results demonstrated that, compared to crimp-balanced woven fabrics, crimp-imbalanced woven fabrics can achieve greater energy-absorption capacities for both normal and oblique impacts. They further showed that crimp imbalance can minimize stress-wave reflections at the crossover regions and can positively alter the spatial and temporal behaviors of stress wave propagations within the fabrics.

Sadegh and Cavallaro[16] developed analytical solutions on the mesoscale of single-ply woven fabrics to assess the effects of crimp contents and yarn friction on energy-absorption capacities and residual projectile velocities. Using work and energy principles, they calculated yarn pull-out and migration forces. Their analytical results further revealed that crimp imbalance can increase the energy-absorption capacities in woven fabrics.

Crimp contents, which are direct results of the selected weave styles and yarn tensions developed during weaving, continue to be investigated for potential performance advantages. Likewise, CG laminates (defined as laminates constructed with a mixture or hybrid of weave styles to achieve a gradient of crimp properties across the laminate thickness) may be used to increase both damage-tolerance thresholds and energy-absorption capacities.

This report documents the research that investigated the effects of weave styles and CGs on the damage-tolerance levels and energy-absorption capacities of WFRP composites. A comparative study was conducted to determine the specific failure mechanisms including fiber/matrix cohesive failures, matrix cracking, fiber breakage, and fiber buckling resulting from static and dynamic loading events.

3. COMPARATIVE STUDY

A comparative study was conducted to measure the effects of laminate weave styles and CG on the mechanical performance, damage tolerance, failure mechanisms, and energy-absorption capacities of woven Kevlar/epoxy laminates. Tests included quasi-static flexure tests of pre-damaged and non-damaged (baseline) laminates, short beam shear tests, low-energy drop impact tests, and ballistic impact tests. Additional experiments were performed using the split Hopkinson compression bar (SHCB) test method to measure dynamic compression properties as functions of laminate weave styles and CG. These properties included in-plane stress-wave speed c_s, in-plane elastic modulus E_{11}, through-thickness elastic modulus E_{33}, and transverse normal strain rates at failure $\dot{\varepsilon}_f$.

3.1 SPECIMEN DESIGN AND FABRICATION

Three weave styles were sourced: plain, 2x2 twill, and 4H satin weaves with DuPont's Kevlar KM2 Plus fiber (a high-performance para-aramid developed for use in military body armor vests and helmets). The weave styles, each of which was obtained in the greige (untreated) state, are shown in figure 1. The mechanical properties of the Kevlar KM2 Plus yarns are listed in table 1. Additional data describing the fabric weave styles and crimp contents are provided in table 2. The warp and weft yarn crimp contents (C_{warp} and C_{weft}, respectively) of each weave style were measured in accordance with ASTM-D-3883-04[17] and were relatively low. Additionally, the fabrics were crimp balanced as the crimp ratio ξ, defined as C_{warp}/C_{weft}, was approximately equal to 1.0 for each weave style.

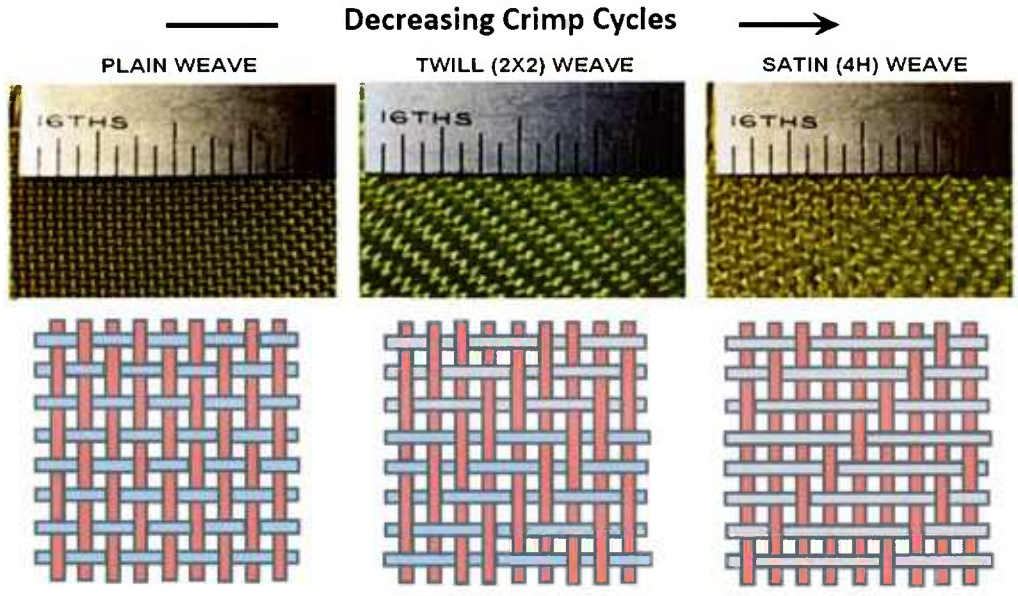

Figure 1. Kevlar Woven Fabric Styles

Table 1. Nominal Mechanical Properties of Kevlar KM2 Plus Yarns

Property	Value
Linear Density	600 denier
Tenacity	28.4 gpd
Breaking Strength	166.8 N
Elongation at Break	3.8%
Elastic Modulus	660.0 gpd

Table 2. Kevlar KM2 Plus Fabric Weave Styles and Properties

Weave Style	Plain	Twill 2x2	Satin 4H
Yarn Denier (warp/weft)	600/600	600/600	600/600
Warp/Weft Counts (yarns/10 cm)	122 x 122	122 x 122	122 x 122
Areal Density (g/m^2)	163.4	163.1	163.8
Fabric Thickness (mm)	0.22	0.20	0.21
C_{warp}(%)	1.6	1.2	1.2
C_{weft}(%)	1.6	1.2	1.2
ξ	1.0	1.0	1.0
Fabric State	Greige	Greige	Greige

Four different laminates, each containing 20 layers of Kevlar fabric, were manufactured. Three laminates were constructed of a single-weave style. The fourth laminate was constructed with hybridized weave styles arranged in a CG manner as $(3\text{-plain}/4\text{-twill}/3\text{-satin})_{SYM}$ and was designated "hybrid CG." Although the term *hybrid* in the field of composites generally refers to a mixture of materials, in the present research, *hybrid* describes a mixture of weave styles. The fabrics were stacked with consistent alignment of the warp and weft axes. A room-temperature, wet lay-up compression molding process was used with a thermoset epoxy resin. Mechanical stops were employed in the mold to achieve approximate fiber volume fractions of 47% – 50% for each laminate.

The hybrid CG laminate was specifically formulated to evaluate its potential to improve the overall combination of strength, stiffness, damage tolerance, and energy-absorption capacity; it is analogous to the process known as case hardening used to harden and strengthen the outer surfaces of metals. The outer plain-woven layers had the highest number of crimp cycles per unit length and were expected to enhance damage tolerance levels (at the cost of strength and stiffness) by restricting in-plane crack propagations to within the length of a single-crimp cycle. The intermediate and central core twill and satin layers, respectively, contained less crimp cycles per unit length and were expected to enhance the stiffness, strength, and dynamic energy dissipation (at the cost of damage tolerance). Performance of the resulting hybrid construction was expected to outperform the plain-woven laminate. Note, however, that the selected hybrid CG construction was merely one of many combinations possible and that further research on other hybrid CG constructions is recommended for additional performance improvements.

The crimped profiles of the warp and weft yarn families for each laminate construction are shown in the micrographs in figure 2. Yarn cross sections were lenticular in shape; layer alignment variations known as nesting were evident for each laminate. Note that a resin-rich region (defect) was observed near the neutral axis of the plain-woven laminate. The weft micrograph of the hybrid CG laminate best captured the through-thickness crimp gradient.

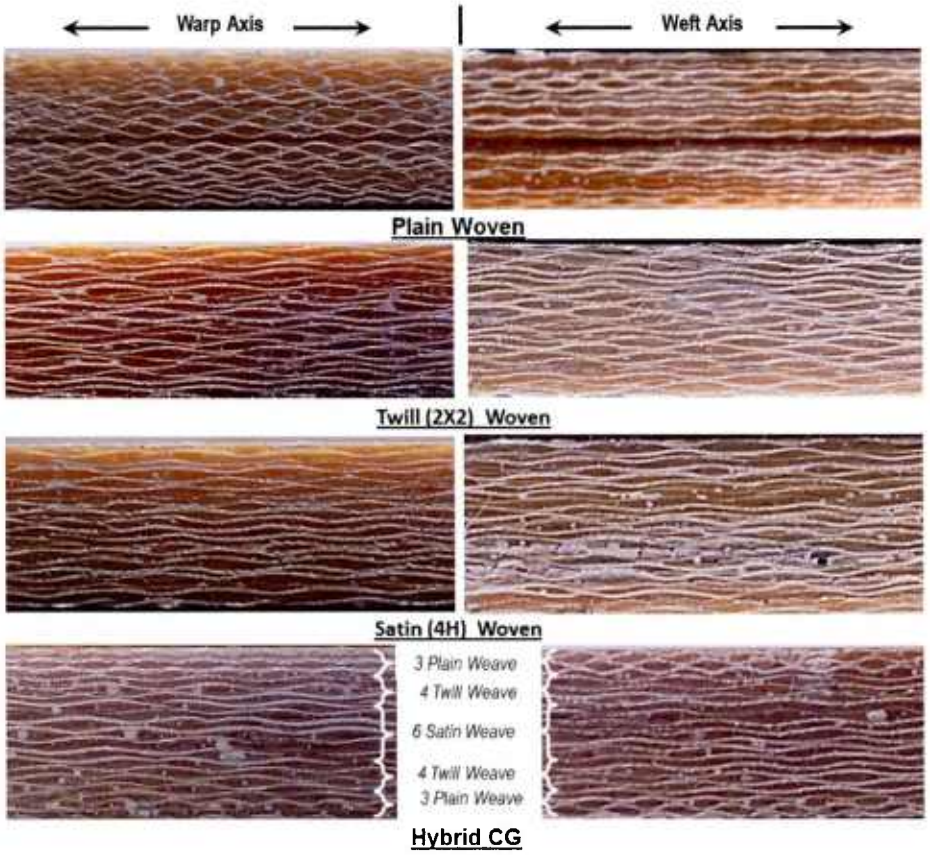

Figure 2. Laminate Through-Thickness Section Views

3.2 SHORT BEAM SHEAR TESTS

Short beam shear tests were conducted to measure the ILSSs of the Kevlar/epoxy laminates as functions of weave styles and crimp gradient. The ILSS is a measure of the cohesive bond strength between adjacent layers. A three-point bend fixture of the type recommended by ASTM Standard D 2344[18] was used as shown in figure 3 in conjunction with an Instron machine. Loading was applied in displacement-control mode at a crosshead rate of 1.27 mm/min. Tests were performed on laminate specimens having nominal thicknesses of 4.8 mm and two different widths, nominally 4.32 mm and 9.65 mm.

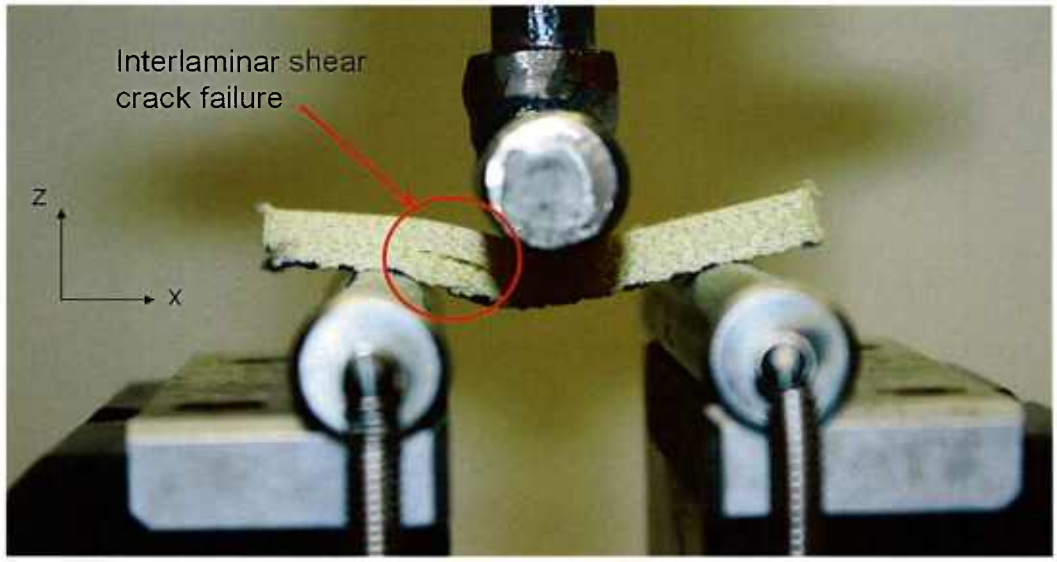

Figure 3. Short Beam Shear Test Fixture and Hybrid CG Specimen Shown with Interlaminar Shear Crack Failure

The interlaminar shear stress σ_{zx} is one of the several weak directional stress components and, when computed in accordance with equation (1), is valid at the laminate neutral plane for specimens having rectangular cross sections. The laminate neutral plane is the location of maximum shear stress and is, therefore, the expected site for initiating cohesive delaminations and matrix shear failures. The ILSS is the maximum value of σ_{zx} achieved.

$$\sigma_{ZX} = \frac{3P}{4A}, \tag{1}$$

where P is the total applied load and A is the cross-sectional area of the specimen.

The averaged ILSSs are shown in figure 4. The plain-, twill-, and satin-woven laminates are presented in order of decreasing crimp cycles along with the hybrid CG laminate. The ILSSs, which clearly exhibited dependence on crimp cycles, increased with decreasing crimp cycles for the non-CG laminates. The plain-woven laminate provided the least ILSS. It is hypothesized that (1) the increased quantity of crimp cycles in the plain-woven laminate produced a corresponding increase in potential cohesive crack initiation sites, (2) the effects of localized mixed-mode fractures (modes I and II) were greater because the plain-woven yarns contained the largest crimping angle of the woven architectures considered, and (3) the transverse shearing deformations increased with increasing crimp cycles, a known source of added shearing compliance, causing the observed reduction in ILSS for the plain-woven laminate. The hybrid CG laminate outperformed all other laminates, yielding a significant 23% increase over the plain-woven laminate. The typical interlaminar shear failure mode shown in figure 3 was a delamination (cohesive failure) at the fiber/matrix interface originating near the laminate neutral plane where the maximum value of σ_{zx} was produced. The delamination did not occur at the resin-rich region of the plain-woven specimen shown in the micrograph of figure 2.

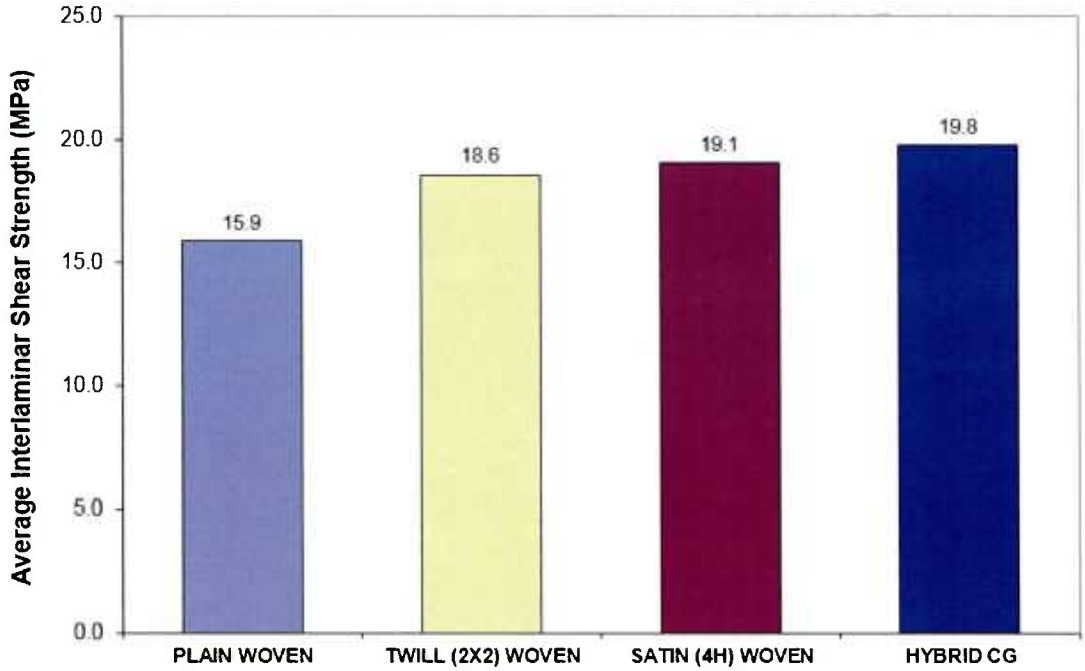

Figure 4. Average Interlaminar Shear Strengths Versus Laminate Constructions

Kim and Sham[2] discussed the positive influence of resin-rich regions on plastic yield zones ahead of crack tip delaminations.

Further inspection of the damage zone shown in figure 5 revealed that multiple failure mechanisms occurred including fiber buckling, shear banding (that is, narrow band of matrix crazing due to stress softening), matrix cracking, and interlaminar shear cracking. Matrix cracking occurred within the weft yarn fiber bundles located along the shear banding region (path A→B) and terminated at the interlaminar shear crack. Fractures in the weft yarn fiber bundles were consistent with those observed for laminate tests performed by others.[3, 4, 10]

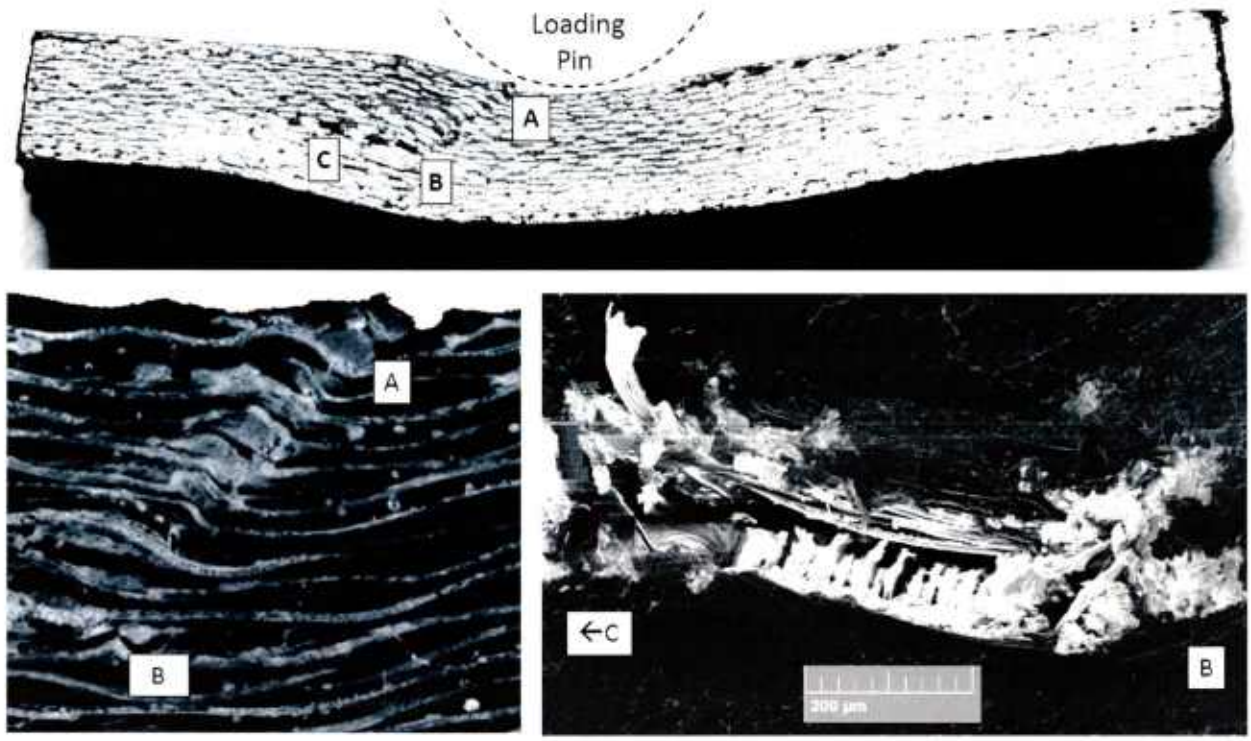

Figure 5. Failure Mechanisms and Damage Zone Paths for Hybrid CG Short Beam Shear Test Specimen: Fiber Buckling on Compressive Surface above Point A, Shear Banding and Matrix Cracking in Weft Yarns along Path A→B→C, and Interlaminar Shear Delaminations with Matrix Crazing along Path B→C

3.3 FOUR-POINT FLEXURE TESTS

Four-point flexure tests were performed on the Kevlar/epoxy laminates to (1) measure the dependence of flexure strength as functions of weave style and CG and (2) baseline the flexure strengths for subsequent comparison to those of pre-damaged laminates (discussed in section 3.5).

A four-point flexure loading fixture with cylindrical steel rollers was used in conjunction with an Instron machine. The diameter of the rollers was 12.7 mm. Loading was applied in displacement-control mode at a crosshead rate of 1.27 mm/min. The load point span L_{LP} and support point span L_{SP} were 38.1 mm and 114.3 mm, respectively. The nominal specimen width and thickness dimensions were 26.0 mm and 4.8 mm, respectively.

The bending stress versus load point displacement δ_{LP} curves are plotted in figure 6. The baseline flexure strengths of the non-CG laminates increased with decreasing crimp cycles. As expected, the baseline flexure strength of the hybrid CG laminate exceeded that of the plain-woven laminate. The baseline flexure strengths among the twill, satin, and hybrid CG laminates exhibited minor variations and collectively averaged 250.03 MPa. The plain-woven laminate, however, exhibited the lowest average baseline flexure strength (186.59 MPa) of all laminates. The hybrid CG laminate provided a 31.3% increase over the plain-woven laminate.

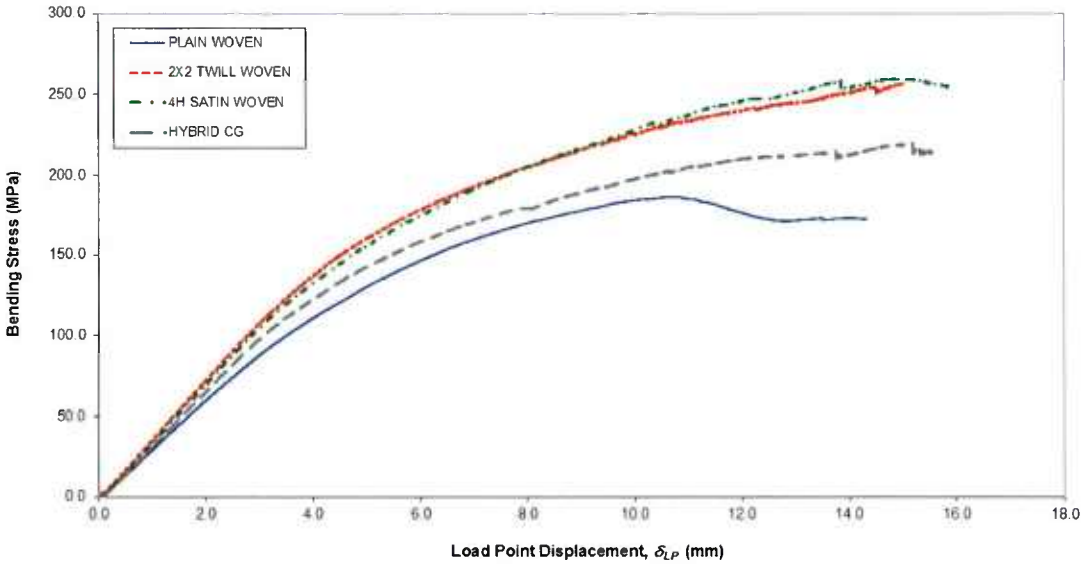

Figure 6. Bending Stress Versus Load Point Displacement Curves for Baseline Flexure Tests

The effect of possible weaving damage on the *as-woven* yarn tensile strengths was addressed to determine if such damage contributed to the low baseline flexure strengths observed for the plain-woven laminates. The plain weave contained the highest number of crimp cycles per unit length among the three weave styles and was therefore expected to incur the most damage. Warp and weft yarns were extracted from fabrics of each weave style and subjected to tension testing. The averaged as-woven tensile strengths are listed in table 3. The results indicated that the warp yarns of the plain weave were nominally weaker by 4.0% with respect to the weft yarns; however, the warp yarn strengths were nearly identical across each weave style. These results confirm that yarn damage from weaving was not a major contributor to the lower baseline flexure strengths measured for the plain-woven laminates; however, the consistency of the as-woven yarn tensile strengths across each tested weave style strongly suggests that the difference in laminate flexure strengths was driven by the crimp contents. It is further hypothesized that increasing crimp contents increases the mixed-mode fracture effects (modes I and II), especially in the plain-woven laminates. Mixed-mode fracture effects on delaminations in composite laminates were investigated by Reeder[12]using experiments on carbon/epoxy and carbon/thermoplastic composites and by Camanho and Davilia[13] using simulations with correlations to experimental data.

Table 3. Average Tensile Strengths of As-Woven Yarns

Weave Style	Warp Yarn Tensile Strength (N)	Weft Yarn Tensile Strength (N)
Plain	152.17	159.29
Twill (2x2)	159.78	158.18
Satin (4H)	154.71	156.40

As shown in figure 6, flexure stiffness began to gradually decrease beyond $\delta_{LP} = 2.54$ mm as nonlinearities developed as a result of stress softening (reduced tangent modulus) of the epoxy matrix, increased shearing deformations, and accumulation of damage. An effective flexure modulus E_{flex} was semi-empirically computed by using Bernoulli-Euler Beam theory (BEBT)[19] to provide the relationship between the measured load point displacements δ_{LP} and E_{flex},as shown in equation (2).

$$E_{flex} = \frac{Pa}{12\delta_{LP} I}\left(4a^2 - 3La\right), \tag{2}$$

where P = total applied load, a = moment arm, L = supported span length, I = moment of inertia of cross section, and δ_{LP} = load point displacement.

Note that BEBT assumes linear elastic material behavior and excludes the effects of transverse shearing deformations δ_{SHEAR} on total deflections, as is expressed in equation (3)

$$\delta_{LP} = \delta_{BEND} + \delta_{SHEAR},$$

$$\delta_{SHEAR} = 0,$$

$$\therefore \quad \delta_{LP} = \delta_{BEND}, \tag{3}$$

where δ_{BEND} and δ_{SHEAR} are the bending and shearing components of total displacement at the load points, respectively.

The resulting values of E_{flex} represented the initial linear responses, as measured at the reference position (δ_{LP} = 2.54 mm) (refer to figure 6), are plotted in figure 7. This reference position was selected because the curves were generally linear up to (δ_{LP} = 2.54 mm) and the corresponding loads were not expected to generate sizable geometric nonlinearities (that is, load-stiffening effects) and shearing deformations, so that $\delta_{LP} \approx \delta_{BEND}$. Figures 6 and 7 clearly depict the effect of increased compliance on E_{flex} for the plain-woven laminate. The hybrid CG laminate yielded an E_{flex} that was 9.7% greater than the E_{flex} of the satin-woven laminate and an E_{flex} that was 27.0% greater than the E_{flex} of the plain-woven laminate.

The observed increases of laminate flexure strength and stiffness with decreasing crimp cycles, as shown in figures 6 and 7, were consistent with the woven laminate uniaxial tensile test results provided by Karahan and Karahan.[8] Similarly, the observed increases in laminate flexure stiffness with decreasing crimp cycles were also consistent with the woven laminated plate flexure test results obtained by Alemi-Ardakani et al.[11]

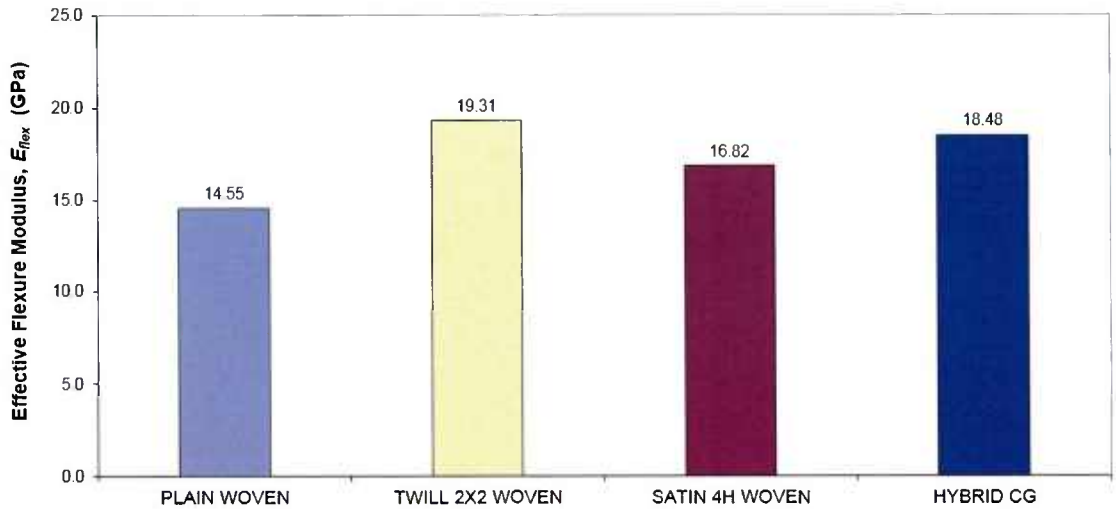

Figure 7. Flexure Modulus E_{flex} Values Semi-Empirically Computed at δ_{LP} for Baseline Laminates

3.4 DROP IMPACT TESTS

The ability of WFRP laminated composites to absorb impulsive forces caused by low-energy impacts is of significant interest to the composites community. The weak-directional stresses previously discussed enable the evolution of damage zones that are often larger in size for composites than for metals. Consider that damage caused by complete through-penetrating impacts, which can be readily detected by eye, can have less effect on structural integrity than non-penetrating impacts. Non-penetrating impacts can produce subsurface delaminations[2] larger than those developed from through-penetration damage; moreover, when subjected to cyclic loads, these subsurface delaminations caused by non-penetrating impacts can grow farther than those caused by through-penetration damage. The aircraft industry, which defines impact damage that may be undetectable by eye as barely visible impact damage (BVID), uses a variety of nondestructive inspection (NDI) techniques to detect the presence of subsurface delaminations. Detection of BVID is important because subsurface damage and unstable crack growth rates can lead to catastrophic structural failures.

Impact behaviors of the Kevlar/epoxy WFRP laminates at the BVID level were assessed using the Instron Dynatup (model 9210) drop test machine. Rectangular specimens of the same geometry used in the previous four-point bend tests were impacted to (1) produce mechanical damage at BVID levels, (2) measure and compare the impact forces, impulses generated, and time duration of loading as functions of weave styles and CG and (3) pre-damage the specimens for the four-point-flexure after-impact tests.

The drop impact test arrangement was a dynamically loaded three-point flexure setup as shown in figure 8. The test was designed to generate multiple damage mechanisms including matrix cracking, fiber buckling, fiber breakage, interlaminar shear, and fiber/matrix delaminations. The rigid mass impactor was a 6.35-mm-radius semicircular cylindrical profile and was instrumented with accelerometers to record the impact force versus time histories. The

50.8-mm-supported span was intentionally shorter than the 114.3-mm-supported span used in the four-point flexure tests. The shorter span was necessary to ensure that the impact damage was confined within the 114.3-mm-support span used in the subsequent four-point flexure after-impact tests.

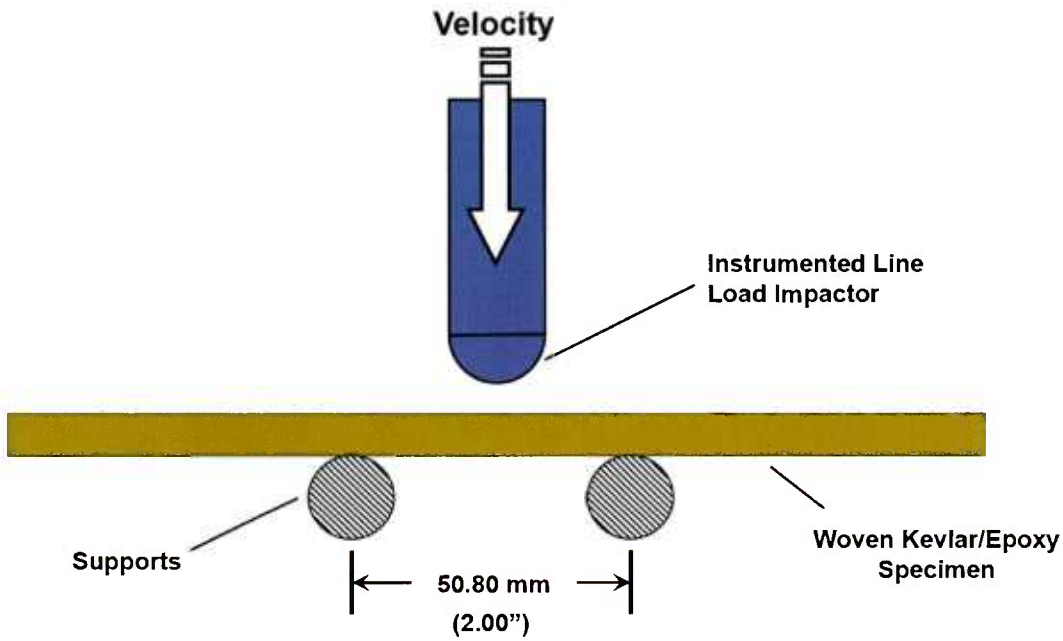

Figure 8. Drop Impact Test Using Three-Point Loading Fixture

Several trial runs were conducted at various energy levels to establish an acceptable energy threshold (AET) for producing damage commensurate with BVID levels. The desired AET was required to generate (1) permanent deflections on the order of the specimen thickness, (2) localized matrix cracking, (3) fiber buckling at the region of impact, and (4) minimal or no fiber breakage on the back face. The selected AET for all subsequent drop impacts was 11.4 J.

The impact damage zones, shown in figure 9 for each laminate, were considered appropriate for BVID levels. Permanent deformations were observed on the order of the laminate thicknesses; fiber buckling occurred within the regions of impact; and minor fiber-tensile failures, which were observed on the back face of several specimens. Figure 10 plots the impact force time histories for each laminate. The hybrid CG produced the maximum impact forces averaging 3737 N followed by the satin laminates, which averaged 3536 N. The averaged impact forces of the twill- and plain-woven laminates were 3136 N and 3025 N, respectively.

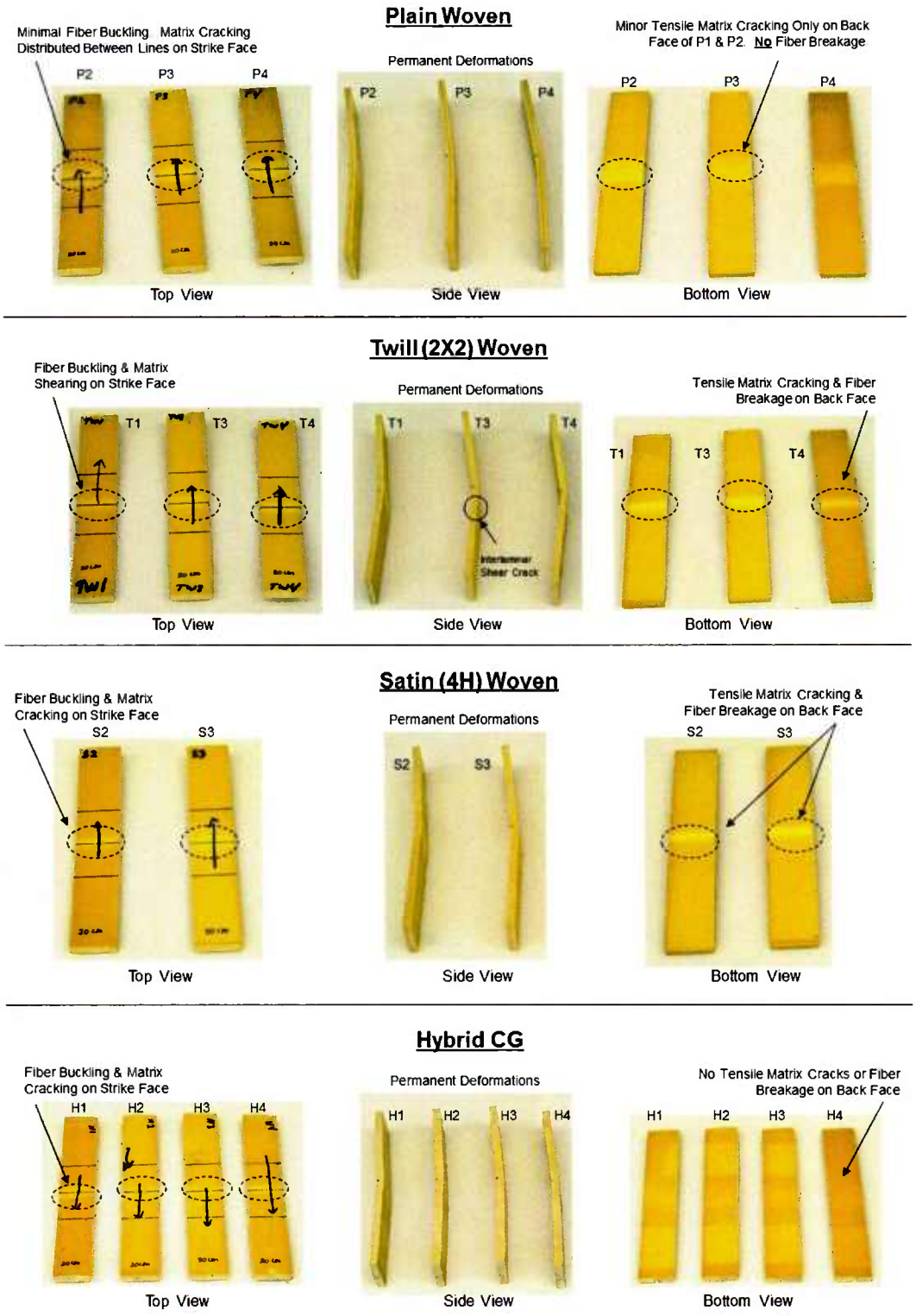

Figure 9. Damage Zones and Deformations from Drop Impact Tests (AET = 11.4 J)

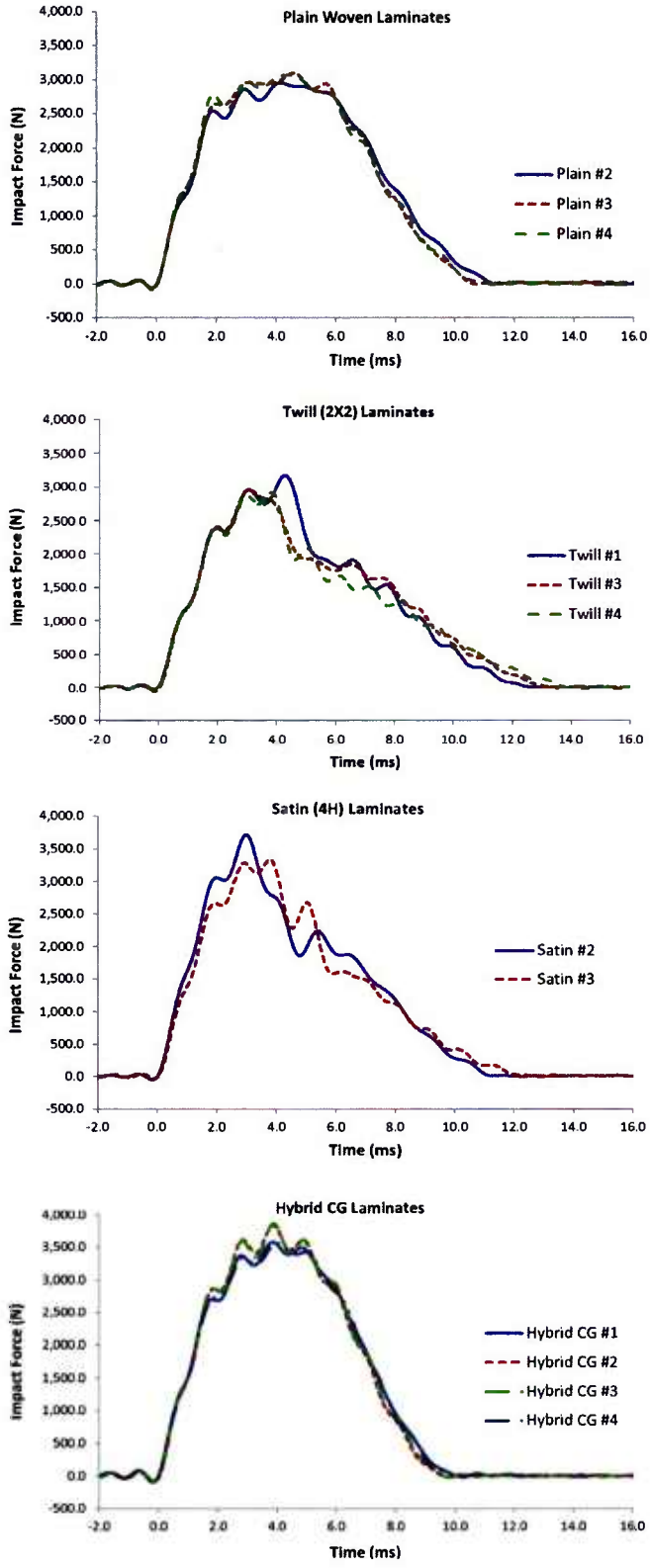

Figure 10. Impact Force Versus Time Histories of Drop Impact Test Specimens (AET = 11.4 J)

The area under each impact force time history curve represents the impulse produced. Impulse quantities can also be computed from the Impulse-Momentum Relationship expressed in equation (4):

$$Impulse = m_{impactor}\left(v_{impact} - v_{initial}\right) = \int_0^t F dt, \tag{4}$$

where $m_{impactor}$ is mass of the falling impactor, v_{impact} is drop velocity at time of impact, $v_{initial}$ is the initial drop velocity (= 0), F is the impact force, and t is time.

Plots of the impulse time histories are shown in figure 11. The times of average loading duration t_{ALD} were computed by averaging the times required for each laminate configuration to achieve their maximum impulse value. The shortest time of average loading duration t_{ALD} was 9.1 ms, which corresponded to the hybrid CG laminates. This observation indicates that the hybrid CG laminates retained the highest stiffness and incurred the least damage of all the laminates tested: the twill- and satin-woven laminates exhibited higher damage levels and longer values of t_{ALD}.

The shapes of the impact force and impulse time history curves provide insight in determining if specimen damage occurred. The lack of symmetry (reflective or asymmetric) indicates that damage was produced. Note the variations in the times of average loading durations t_{ALD} among all laminate constructions and compare the initial portions of the impulse curves to the regions ending at t_{ALD}. The presence of damage increased t_{ALD}.

3.5 FOUR-POINT-FLEXURE AFTER-IMPACT TESTS

The objective of the four-point-flexure after-impact tests was to assess damage tolerance in bending at the BVID level. These tests were performed using the same bending arrangement and loading rate described in section 3.3. Here, the residual flexure strengths of laminates containing drop impact damage (AET = 11.4 J) were measured and compared to assess the effects of weave styles and crimp gradient.

The residual and baseline flexure strengths are shown in figure 12. The plain-woven and hybrid CG laminates exhibited significantly high damage-tolerance levels by retaining 98% and 94% of their baseline strengths, respectively. In contrast, the twill and satin laminates incurred greater damage, demonstrating lower damage-tolerance levels by retaining only 72% and 71% of their baseline strengths, respectively. Figure 12 also demonstrates that the residual flexure strengths of the twill and satin laminates for an AET of 11.4 J reduced to approximately the baseline strength of the plain-woven laminate.

The residual flexure strengths decreased linearly with increasing t_{ALD} as shown in figure 13. Comparing the extreme residual flexure strengths, on average, the hybrid CG laminates outperformed the satin-woven laminates by 28%. The hybrid CG laminate designs clearly demonstrated combined higher baseline flexure strengths and damage-tolerance levels and are therefore recommended for use in critical composite structures over non-CG laminates.

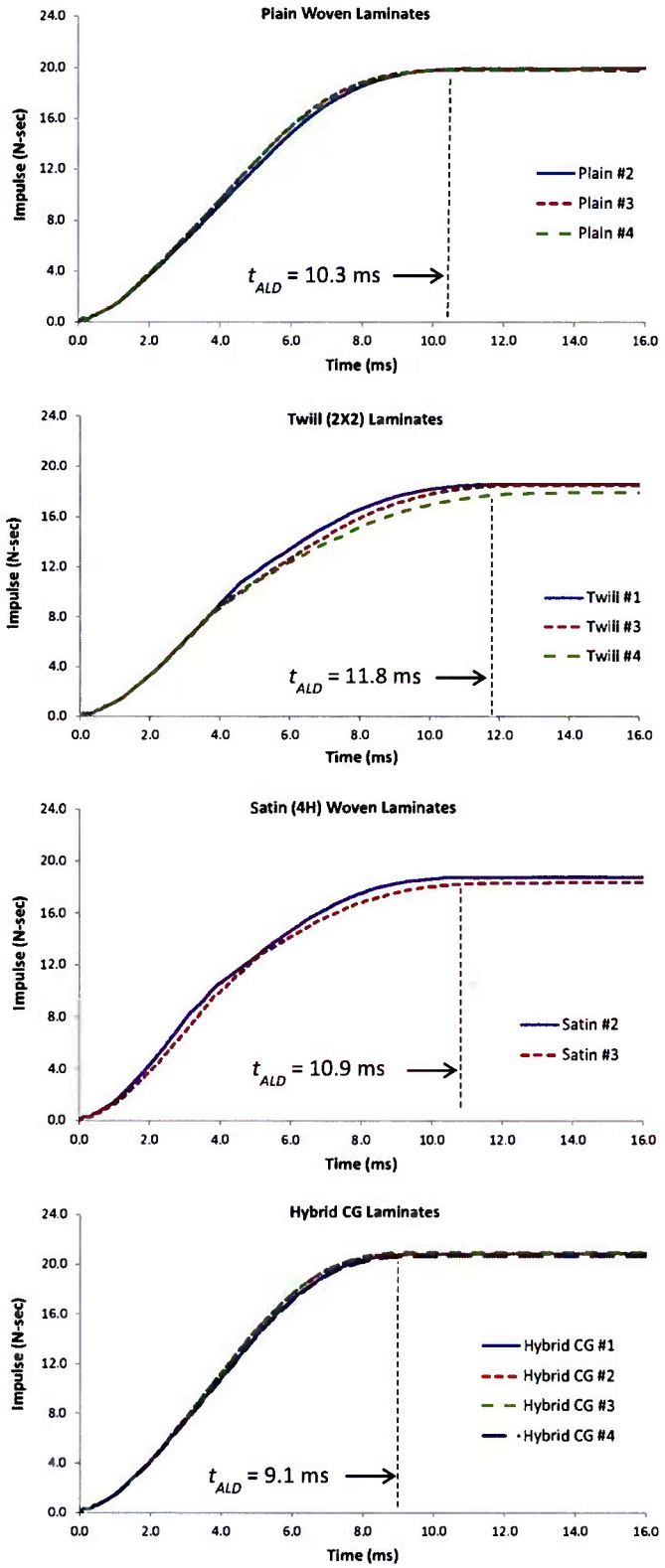

Figure 11. Impulse Time Histories of Drop Impact Test Specimens (AET = 11.4 J)

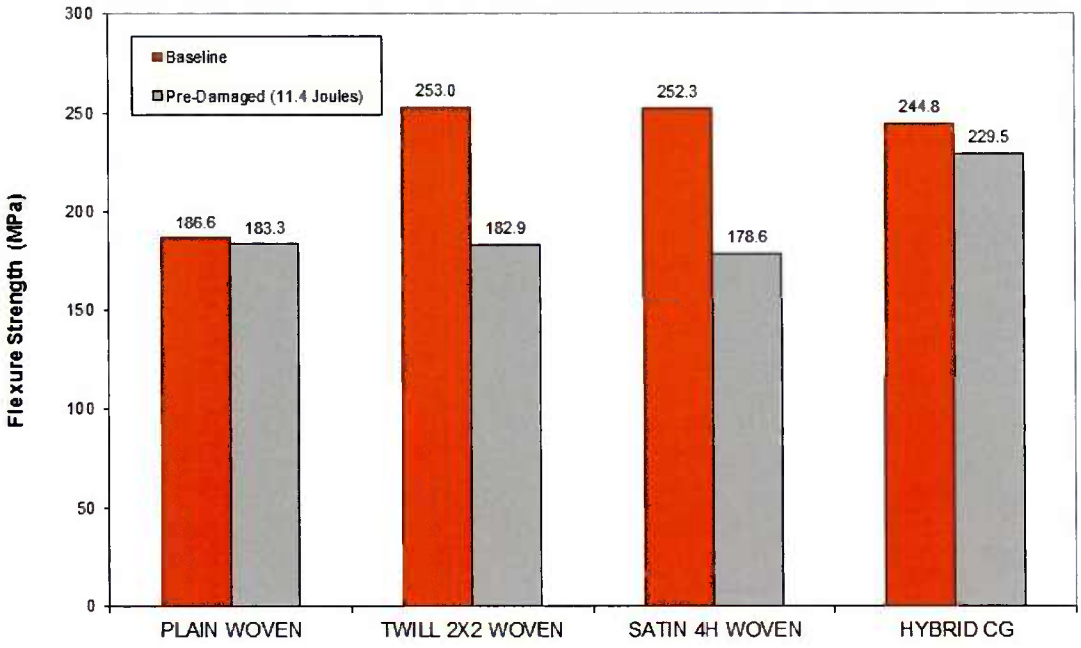

Figure 12. Comparison of Four-Point Bend Baseline and Pre-Test Impact Damaged Flexure Strengths (AET = 11.4 J)

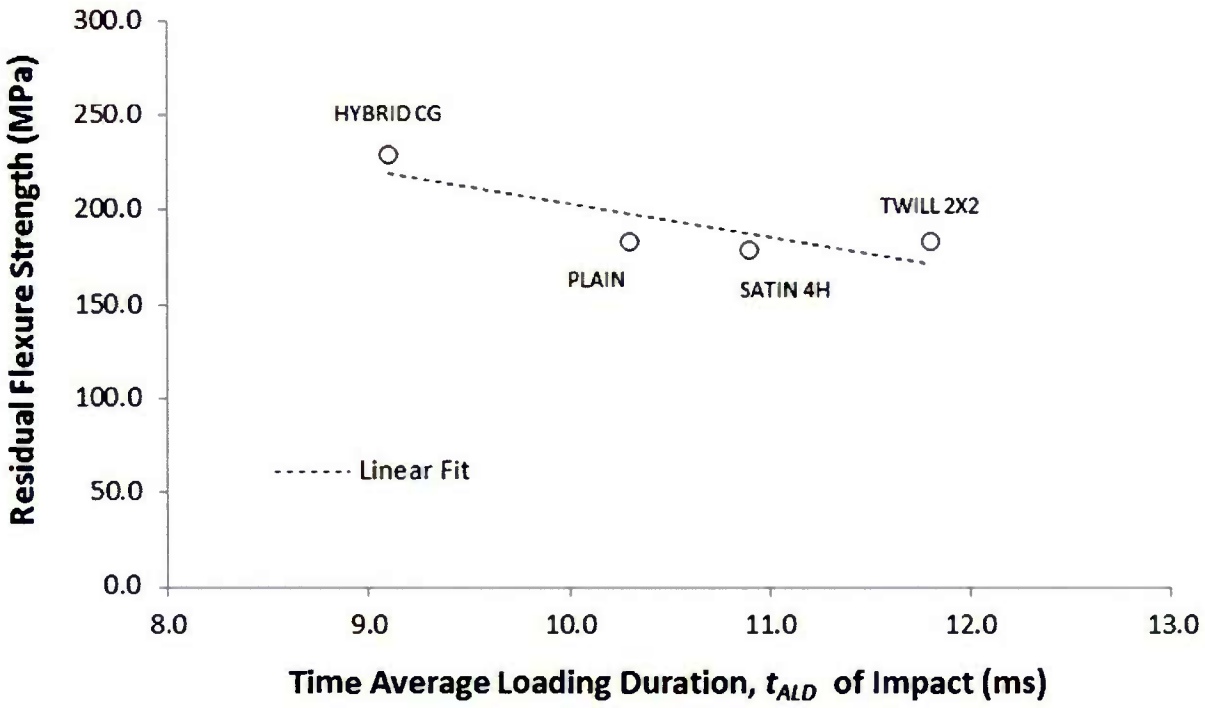

Figure 13. Residual Flexure Strengths Versus t_{ALD} (AET = 11.4 J)

3.6 WAVE SPEED MEASUREMENT TESTS

The use of different weave constructions and CGs to selectively influence the transmission of stress waves within WFRP laminates was investigated as a possible approach to increasing dynamic energy-absorption capacities and damage-tolerance levels.

Stress waves in a given material travel at velocities equivalent to the speed of sound in that material. The sound speed (or wave speed) c_s is related to several properties of the material as shown in equation (5):

$$c_s = \sqrt{\frac{E(1-\nu)}{\rho(1+\nu)(1-2\nu)}}, \tag{5}$$

where E is Young's Modulus, ν is Poisson's Ratio, and ρ is mass density.

A series of SHCB experiments was performed on the laminate specimens to measure their in-plane stress-wave velocities along the warp directions as functions of weave styles and CG. The experimental setup and specimen dimensions are shown in figures 14(a) and 14(b). Using a compressed air chamber (not shown), a striker bar is propelled toward the incident bar. When the striker bar impacts the incident bar, a compressive stress wave is generated. This wave travels through the incident bar and splits into two stress waves—one is the reflected wave, which returns back into the incident bar, and the other is the transmitted wave, which travels through the specimen and into the follower bar. The amount of energy associated with the reflected and transmitted waves depends on the impedance mismatch of the bar and specimen materials. The specimen absorbs the dynamic energy in both elastic and inelastic forms. The elastic (recoverable) energy is transmitted to the follower bar; the inelastic (irrecoverable) energy is dissipated and lost. The energy dissipated by the specimen (that is, through friction, damage, and heat, for example) reduces the relative velocity of the follower bar with respect to the incident bar. Strain gages mounted on the surface of the laminate at the locations shown in figure 14(b) captured the strain time histories of each specimen. This method provided an effective strain time history; it did not characterize the layer-by-layer strain time histories. The stress-wave arrival times were obtained from the strain time histories.

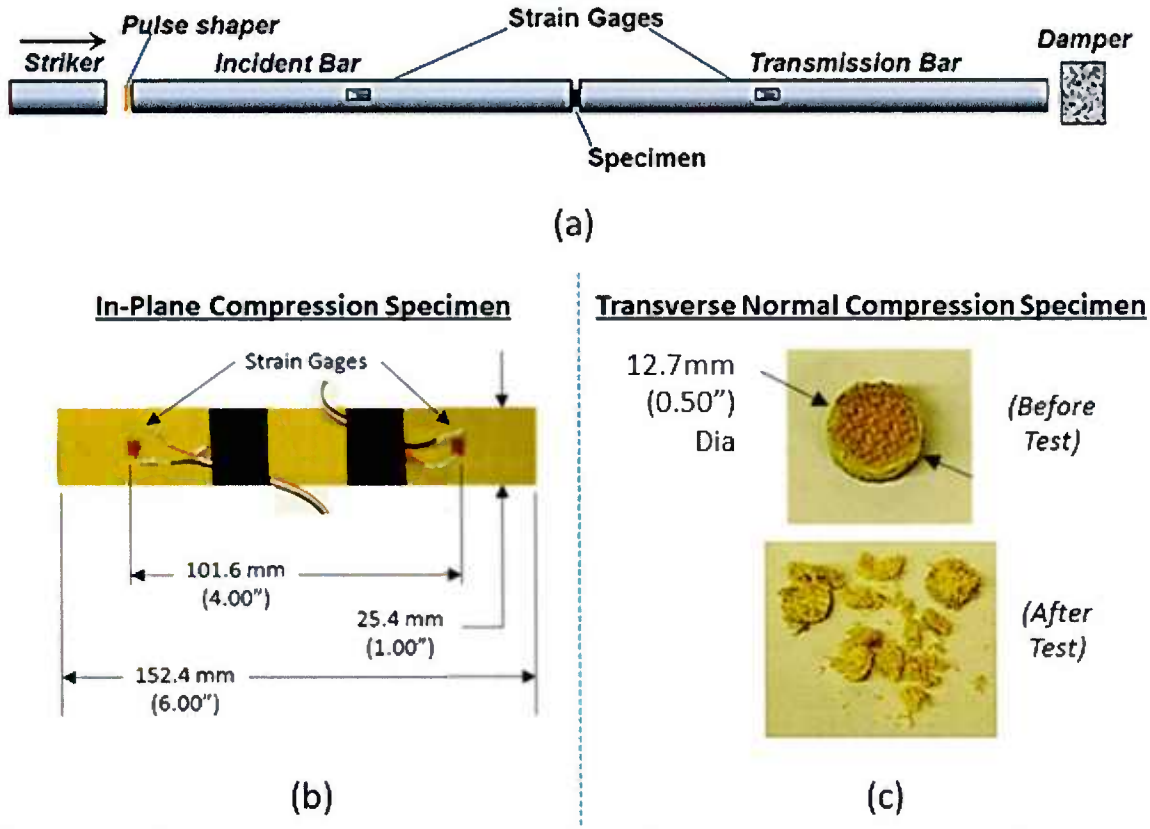

Figure 14. Schematic of SHCB Experiment: (a) SHCB Setup, (b) In-Plane Compression Specimen, (c) Transverse Normal Compression Specimen

The averaged wave speed c_s and in-plane compressive moduli E_{11} (computed using equation (5)) were plotted (see figure 15) and clearly demonstrated dependence on weave styles and CG. The wave speeds and in-plane compressive moduli results were "as expected" with the exception that the twill (2x2)-woven laminates achieved the highest averaged wave speed (4253.7 m/s) followed by the satin (4H)-woven laminates (4055.5 m/s). Similarly, the twill-woven laminates averaged the highest in-plane compressive modulus (22.7 GPa) followed by the satin-woven laminates (20.3 GPa). The observed exceptions can be clarified by reviewing the figure 2 micrographs and comparing the crimp wavelengths measured for both laminate types. Because the warp axis views of the twill and satin laminates exhibited similar crimp wavelengths, comparable wave speeds were measured. The minimum wave speeds and in-plane compressive moduli results were reported for the plain-woven laminates on average (3677.0 m/s and 16.7 GPa, respectively). The plain-woven laminates had the shortest crimp wavelengths as shown in figure 2. The hybrid CG laminates provided an intermediate average wave speed (3976.5 m/s), which was expected using velocity measurements obtained from the surface-mounted strain gages. Comparison of figures 15 and 7 shows that the dynamic in-plane compressive moduli slightly exceeded the static in-plane flexure moduli; both exhibit generally similar dependence on weave styles and CG. The through-thickness gradient profile of the ply-by-ply wave speed for the hybrid CG laminate is analogous to viscous fluid flow through a pipe.

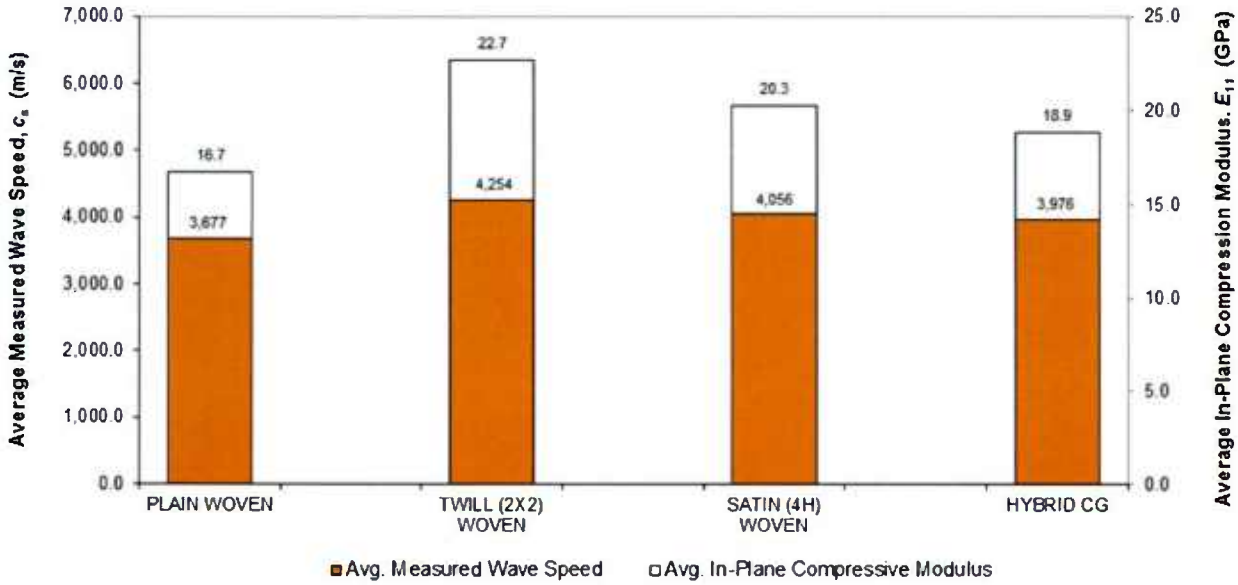

Figure 15. Averaged Wave Speeds and In-Plane Compression Moduli Results Versus Laminate Constructions (Warp Direction)

3.7 DYNAMIC STRENGTH AND STRAIN-RATE MEASUREMENT TESTS

Polymer composites, unlike metals, generally exhibit increased strengths with increasing strain rates. This viscoelastic effect is particularly beneficial for structures designed to support severe dynamic loading events such as blast, ballistic impact, mechanical shock, etc. To take advantage of this viscoelasticity, failure mechanisms and the corresponding strain rates must be identified. Accordingly, the dynamic transverse normal compressive stress-strain behaviors of the woven Kevlar/epoxy laminates were measured using the SHCB test method shown in figure 14(a). The dynamic transverse normal compressive strengths and corresponding strain rates at failure were measured.

The specimens were machined in the form of circular disks having a 12.7-mm nominal diameter as shown in figure 14(c). The diameters of the incident and follower bars were 19.1 mm. The fragmented fracture mode, also shown in figure 14(c), was observed for each of the laminates tested with the dominant failure mechanisms being matrix cracking and delaminations. Plots of true stress σ_{tr} versus true strain ε_{tr} are shown in figure 16 for each laminate configuration. The highest averaged strength was observed for the twill laminate at 675 MPa, and the lowest averaged strength was for the hybrid CG laminate at 502 MPa. The averaged strengths and failure strains were plotted for each laminate construction in figure 17.

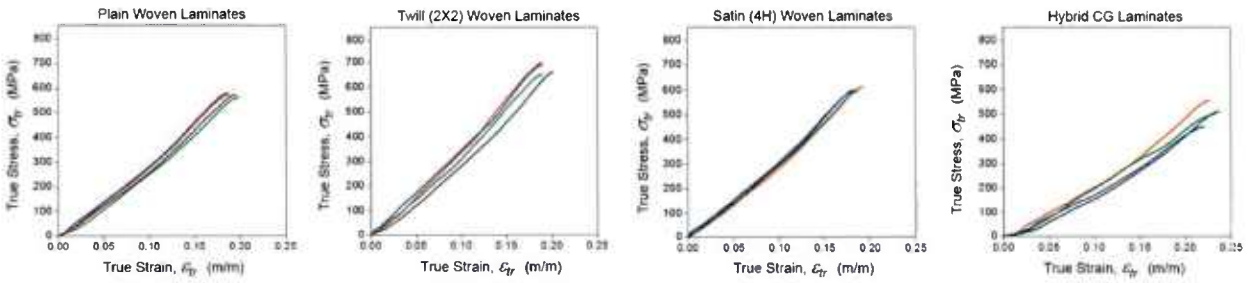

Figure 16. True Stress σ_{tr} Versus True Strain ε_{tr} Plots for Transverse Normal SHCB Tests

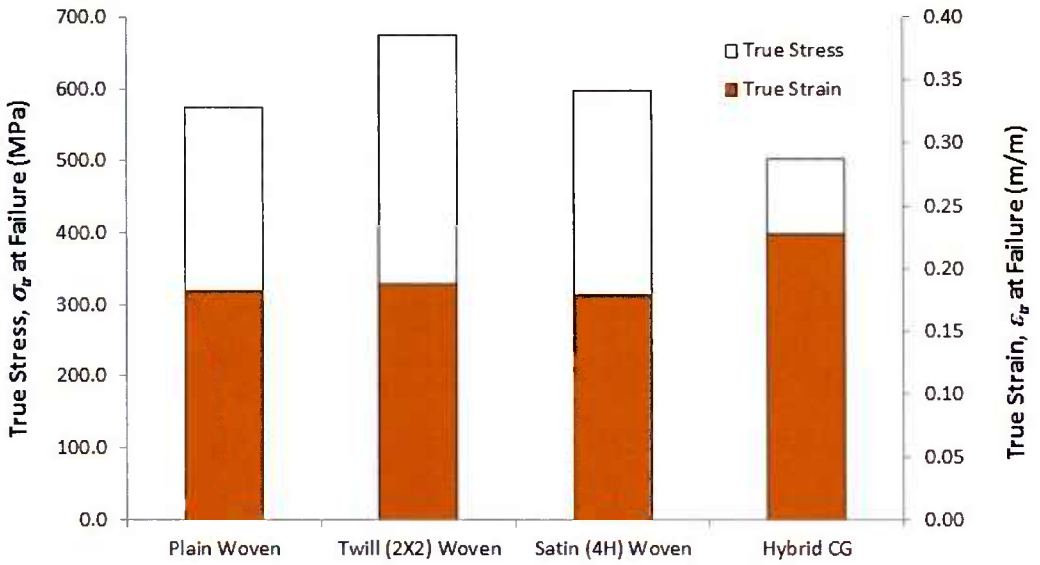

Figure 17. True Stresses σ_{tr} and True Strains ε_{tr} at Failure Versus Laminate Constructions

The dynamic transverse normal compressive strength rankings indicated that the twill and satin laminates were stronger than the plain-woven laminates by 17.4% and 4.0%, respectively; however, the hybrid CG laminates were weaker than the plain-woven laminates by 12.7% on average.

Compared to the average failure strain of the plain-woven laminates, the twill laminate strain was 3.3% higher and the satin laminate strain was 1.6% less. The hybrid CG laminates, however, yielded the highest averaged failure strain overall and exceeded that of the plain-woven laminates by 25.3%. This observation suggests that the hybrid CG laminate may have a greater damage-tolerance level in through-thickness compression than do the plain-, twill-, and satin-woven laminates. Each of the different laminate constructions yielded strain rates at failure $\dot{\varepsilon}_f$ on the order of 4000 s^{-1}.

3.8 BALLISTIC IMPACT TESTS

Ballistic impact testing was performed to measure the ballistic energy absorption capacities of the woven laminates and to identify the damage mechanisms present. Conical steel projectiles having a nominal weight of 6.5 grams and a nominal diameter of 7.87 mm were shot using a gas gun at a normal angle of incidence. The dimensions of the test specimens were 101.6 mm by 101.6 mm. The specimens were clamped in a mounting fixture along their warp edges, thus providing a 63.5-mm by 101.6-mm aperture. Trial tests were performed to determine a minimum projectile velocity range that produced both complete penetration in all laminates and non-zero residual projectile velocities. The objective projectile velocity range was 137.16 m/s to 152.4 m/s. A high-speed digital imaging system recorded each ballistic test at 20,000 frames/second and measured the initial and residual projectile velocities.

Additionally, three stages of the ballistic impact event were captured (see figure 18): pre-impact, impact, and complete penetration stages.

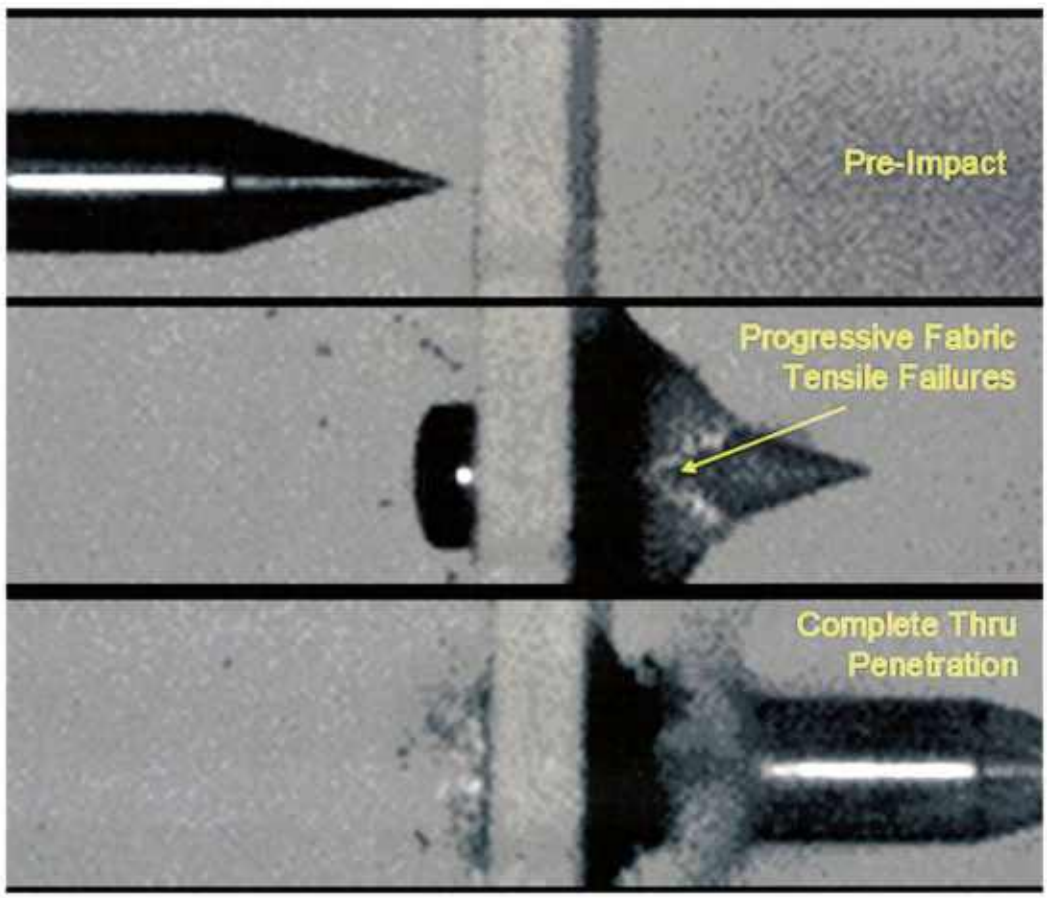

Figure 18. Digital Images for Three Stages of the Ballistic Impact Event

Visual inspections of the damage zones shown in figure 19 revealed three distinctly characteristic failure modes for WFRP composites subject to rigid projectile impacts: (1) diamond-shaped patterns of delaminations were produced on the incident and back faces extending around the projectile hole; (2) cross-like patterns of progressive warp- and weft-fiber tensile failures formed on the back faces; and (3) matrix cracking and fabric-shearing deformations were generated along the off-fiber axes of the back faces. These modes were present in each tested laminate construction.

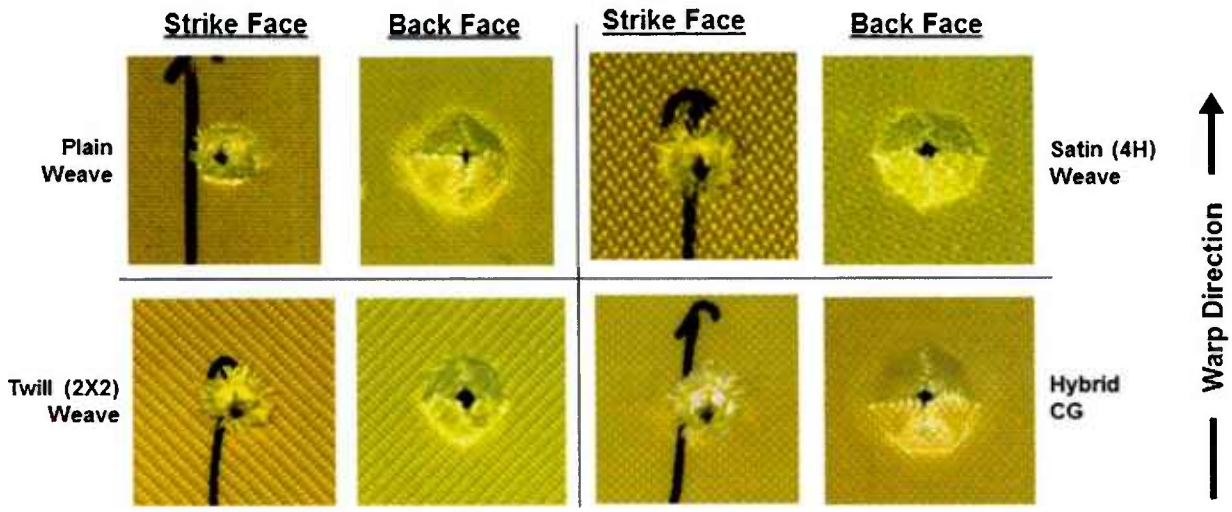

Figure 19. Damage Zones in Ballistic Impact Test Specimens

Microscopic examinations were performed on fractured fibers extracted from the strike and back faces to identify and compare the types of fiber deformations present. Fiber fractures from both faces exhibited fibrillated and elongated deformations, thus confirming that the fractures were tensile in nature. Fibrillated deformations are the most prevalent among the tensile modes known for Kevlar fibers[20] and result from the extrusion-induced anisotropy developed during the fiber-spinning process. The fiber deformations shown were dependent on the conically shaped projectiles used. Other projectile shapes may produce different deformations between strike-face and back-face fibers. For example, right-circular cylinder (RCC) projectiles will likely generate shear and compressive failures of the strike-face fibers and tensile failures of back-face fibers.

The velocity and energy-absorption results are listed in table 4. The averaged energy absorptions for each laminate style are plotted in figure 20. The ballistic impact test results provided the basis for ranking energy-absorption capacities for each of the woven laminate constructions. The satin and hybrid CG laminates outperformed the plain-woven laminate by absorbing nearly 10% and 6% more ballistic energy, respectively. The twill laminate absorbed nearly 3% less energy than the plain-woven laminate. The results, however, were further dependent on the projectile shape, size, and material; target specimen size and fiber volume fractions; mounting fixture; and initial velocities used. Additional ballistic impact tests are recommended using other projectile shapes and other hybrid CG laminate constructions.

Table 4. Velocity and Energy Results of Ballistic Impact Tests

Laminate	Specimen	Projectile Weight (g)	$V_{Initial}$ (m/s)	$V_{Residual}$ (m/s)	ΔV (m/s)	$KE_{Initial}$ (N-m)	$KE_{Residual}$ (N-m)	Energy Absorbed (N-m)	Energy Absorbed (%)
Plain Woven	1	6.53	141.11	76.97	64.14	64.96	19.33	45.63	70.25
	2	6.41	149.41	92.36	57.05	71.49	27.32	44.17	61.79
	3	6.48	149.41	76.97	72.44	72.27	19.18	53.09	73.46
	4	6.51	149.41	87.59	61.82	72.60	24.95	47.65	65.63
	5	6.48	143.77	88.60	55.17	66.92	25.41	41.50	62.02
Twill (2x2) Woven	1	6.37	149.41	88.60	60.81	71.04	24.98	46.06	64.84
	2	6.41	149.41	90.71	58.70	71.49	26.35	45.14	63.14
	3	6.42	141.11	79.38	61.73	63.87	20.21	43.66	68.35
	4	6.5	146.54	88.60	57.94	69.73	25.49	44.24	63.44
Satin (4H) Woven	1	6.48	146.54	74.71	71.83	69.52	18.07	51.45	74.01
	3	6.49	152.40	83.74	68.66	75.31	22.74	52.57	69.81
	4	6.52	143.77	71.21	72.56	67.33	16.52	50.81	75.47
Hybrid CG	1	6.44	146.54	81.94	64.60	69.09	21.60	47.49	68.73
	2	6.54	141.11	73.98	67.13	65.06	17.88	47.18	72.51
	3	6.48	146.54	79.38	67.16	69.52	20.40	49.12	70.66

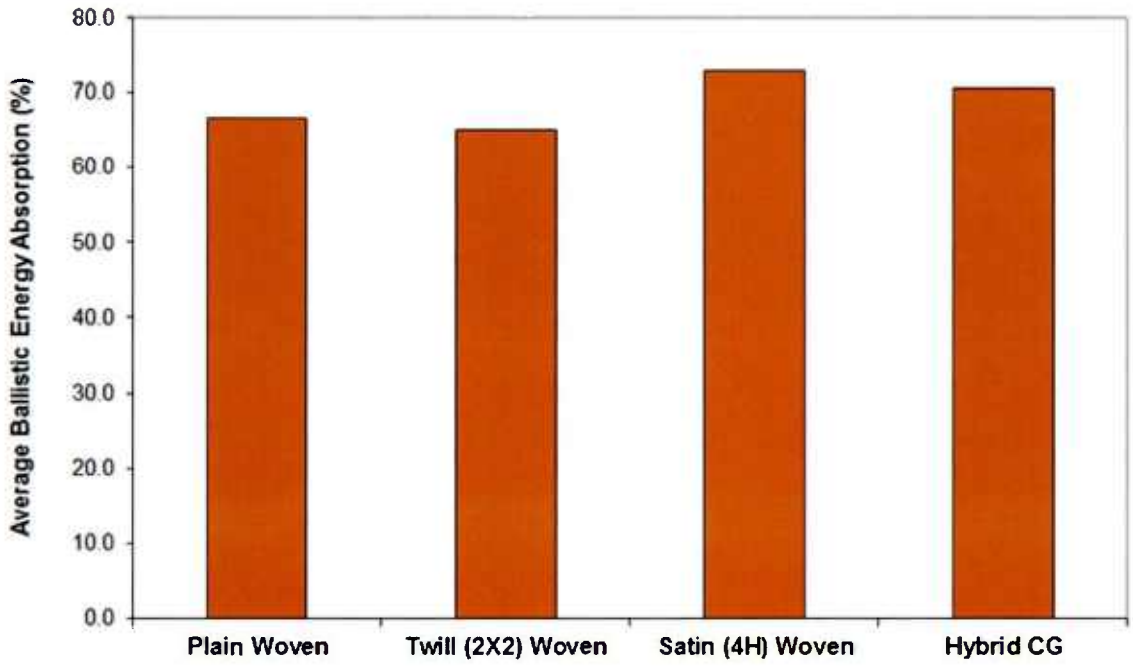

Figure 20. Average Ballistic Energy Absorption Versus Laminate Construction

4. SUMMARY AND CONCLUSIONS

An extensive comparative study was performed on 20-ply woven Kevlar/epoxy laminates. Laminates of three different weave styles were studied. The fabric weaves included plain, twill (2x2), and satin (4H) styles. A fourth laminate was manufactured with a hybrid CG construction consisting of a symmetric mixture of weave styles so that the gradient of crimp cycles per unit length decreased from the outer layers toward the central (core) layers. The crimp contents were balanced between the warp and weft yarns within each weave style. The laminates were experimentally evaluated, and their architectural influence on damage-tolerance levels and energy-absorption capacities was measured.

The experiments yielded the following results:

1. The hybrid CG and satin laminates provided 23% higher averaged ILSS in contrast to the plain-woven laminates as measured from short beam shear tests. Failure modes were dominated by matrix shearing and cracking, buckling of the warp fibers along the compressive surface, and interlaminar shear delaminations.

2. The average baseline flexure strengths of the satin, twill, and hybrid CG laminates exceeded the average baseline flexure strength of the plain-woven laminates by more than 30% and were nearly identical, varying by 0.5%. The average baseline flexure modulus of the twill and hybrid CG laminates exceeded that of the plain-woven laminates by more than 25%. Failure modes included matrix cracking and fiber breakage.

3. The hybrid CG and plain-woven laminates provided greater damage-tolerance levels to BVID at the AET value of 11.4 J and retained significantly higher residual strengths compared to the twill and satin laminates. The hybrid CG produced the maximum averaged impact force followed by the satin-, twill-, and plain-woven laminates. The shortest time of average loading duration t_{ALD} was observed for the hybrid CG laminates indicating that maximum stiffness was retained and the least damage generated. The twill- and satin-woven laminates exhibited higher damage levels and correspondingly longer values of t_{ALD}. The residual flexure strengths were observed to decrease linearly with increasing t_{ALD}. Failure modes included matrix cracking with fiber breakage.

4. The twill laminates provided on average the highest wave speed c_s (4253.7 m/s), followed by the satin (4055.5 m/s), hybrid CG (3976.5 m/s), and plain-woven laminates (3,677.0 m/s) as measured from in-plane SHCB tests. The twill laminates averaged 16% higher wave speed than that of the plain-woven laminates. Similarly, the dynamic in-plane compression modulus E_{11} along the warp directions was highest for the twill laminate and lowest for the plain-woven laminate. The twill-woven laminates exhibited a 30% increase in E_{11} over the plain-woven laminates. The wave-speed measurements clearly show dependence on weave style and CG. The specimens were not loaded to failure.

5. The transverse normal SHCB tests measured the highest compression strength for the twill-woven laminates, followed by the satin, plain, and hybrid CG laminates; however, the highest averaged compressive strain to failure was demonstrated by the hybrid CG laminate, which exceeded that of the plain-woven laminates by 25.3%. This finding suggests that the damage-tolerance level in through-thickness compression for the hybrid CG laminate may be similarly greater than that for the plain-woven laminates. All laminates exhibited approximate strain rates at failure of 4000 s^{-1}. Failure modes were dominated by matrix cracking and delaminations.

6. The ballistic impact tests revealed that the satin-woven laminates absorbed the highest averaged energy (73.1%), followed by the hybrid CG (70.6%), plain-woven (66.6%), and twill-woven (64.9%) laminates. Failure modes included matrix cracking, fabric shearing, delaminations, and fiber breakage. Microscopic inspections of fractured fibers extracted from the strike and back faces showed that tensile failure modes were produced on both faces. These modes generally vary with the shapes of the projectiles used; therefore, ballistic protection devices should be designed to maximize fiber performance and fracture modes for specific projectile threats. Additional ballistic impact tests are needed to identify fiber failure modes for other specific projectile shapes of interest; moreover, additional tests to evaluate alternative hybrid CG laminate constructions are also recommended.

7. The laminate rankings obtained from the quasi-static experiments (short beam shear, flexure) and the high-speed experiments (drop impact, in-plane wave speed, transverse normal SHCB and ballistic impact tests) depended on the type, location, and extent of damage induced; presence of localized mixed mode coupling; and the influence of viscoelastic behaviors during the dynamic experiments. Strength rankings from the ILSS and baseline flexure tests, however, demonstrated nearly identical trends versus laminate architectures. Stiffness rankings from the baseline flexure and dynamic in-plane compression tests also exhibited generally comparable dependence of the in-plane moduli versus laminate architectures.

Results of this research confirmed that damage-tolerance levels and energy-absorption capacities can be increased by optimally tailoring the weave styles and utilizing crimp gradient constructions.

REFERENCES

1. R. M. Jones, "Mechanics of Composite Materials," Hemisphere Publishing Corporation, NY, 1975.

2. J. K. Kim and M. L. Sham, "Impact and Delamination Failure of Woven-Fabric Composites," *Composites Science and Technology*, vol. 60, pp. 745 – 761, 2000.

3. H. Ullah, A. Harland, V. Silberschmidt, "Evolution and Interaction of Damage Modes in Fabric-Reinforced Composites Under Dynamic Flexural Loading," *Composites Science and Technology*, vol. 92, pp. 55 – 63, 2014.

4. H. Ullah, A. Harland, and V. Silberschmidt, "Characterization of Mechanical Behavior and Damage Analysis of 2D Woven Composites Under Bending," *Composites Part B*, vol. 75, pp. 156 – 166, 2015.

5. R. Park and J. Jeng, "Effect of Laminate Geometry on Impact Performance of Aramid Fiber/Polyethylene Fiber Hybrid Composites," *Journal of Applied Polymer Science*, vol. 75, no. 7, pp. 952 – 959, 2000.

6. N. Naik, Y. C. Sekher, and S. Meduri, "Damage in Woven-Fabric Composites Subjected to Low Velocity Impact," *Composites Science and Technology*, vol. 60, pp. 731 – 744, 2000.

7. B. S. Thatte, G. S. Chandekar, A. D. Kelkar, and P. Chaphalkar, "Studies on Behavior of Carbon and Fiberglass Epoxy Composite Laminates Under Low Velocity Impact Loading Using LS-DYNA," *10th International LS-DYNA Users Conference*, Dearborn, MI, June 8 – 10, 2008.

8. M. Karahan and N. Karahan, "Influence of Weaving Structure and Hybridization on the Tensile Properties of Woven Carbon-Epoxy Composites," *Journal of Reinforced Plastics*, vol. 33, no. 2, pp. 212 – 222, 2014.

9. N. K. Naik, R. Ramasimha, H. Arya, S. V. Prabhu, and N. ShamaRao, "Impact Response and Damage Tolerance Characteristics of Glass-Carbon/Epoxy Hybrid Composite Plates," *Composites: Part B*, vol. 32, pp. 565 – 574, 2001.

10. S. Daggumati, I. De Baere, W. Van Paepegem, J. Degrieck, J. Xu, S. V. Lomov, and I. Verpoest, "Local Damage in a 5-Harness Satin Weave Composite Under Static Tension: Part 1 – Experimental analysis," *Composites Science and Technology*, vol. 70, pp. 1926 – 1933, 2010.

11. M. Alemi-Ardakani, A. S. Milani, S. Yannacopoulos, and H. Borazghi, "A Rapid Approach for Predication and Discrete Lay-Up Optimization of Glass Fiber/Polypropylene Composite Laminates Under Impact," *International Journal of Impact Engineering*, vol. 84, pp. 134 – 144, 2015.

REFERENCES (Cont'd)

12. J. R. Reeder, "An Evaluation of Mixed Mode Delamination Failure Criteria," NASA/TM 104210, Langley Research Center, 1992.

13. P. P. Camanho and C. G. Davilia, "Mixed-Mode Decohesion Finite Elements for the Simulation of Delamination in Composite Materials," NASA/TM-2002-211737, Langley Research Center, 2002.

14. P. Cavallaro and A. Sadegh, "Crimp Imbalanced Protective Fabrics," *2010 ASME International Mechanical Engineering Congress and Exposition*, Vancouver, BC, November 12 – 18, 2010, IMECE2010-40610.

15. *ABAQUS/Explicit*, Ver. 6.6, ABAQUS Inc., Pawtucket, RI, 2007.

16. A. Sadegh and P. Cavallaro, "Mechanics of Energy Absorbability in Plain-Woven Fabrics: An Analytical Approach," *Journal of Engineered Fibers and Fabrics,* vol. 7, no.1, pp. 10 – 25, 2011.

17. American Society for Testing and Materials, "Standard Test Method for Yarn Crimp and Yarn Take-Up in Woven Fabrics," ASTM D3883-04, DOI: 10.1520/D3883-04R12.

18. American Society for Testing and Materials, "Standard Test Method for Short-Beam Strength of Polymer Matrix Composite Materials and their Laminates," ASTM D2344/D2344M – 13, DOI: 10.1520/D2344_D2344M.

19. A. Ugural and S. Fenster, "Advanced Strength and Applied Elasticity," Elsevier North-Holland Publishing Co, 2nd ed., 1977.

20. H. H. Yang, "Kevlar Aramid Fiber," John Wiley & Sons Ltd, 1993.

INITIAL DISTRIBUTION LIST

Addressee	No. of Copies
U.S. Army Research Laboratory, Aberdeen Proving Ground, MD (AMSRD-ARL-WM-MD (B. Cheeseman, R. Dooley, C. Yan, B. Scott), RDRL-WMM-D (V. Champagne, Jr.), RDRL-WMP-F (A. Frydman), RDRL-WMM-A (M. Maher))	7
U.S. Army Aberdeen Test Center, Aberdeen Proving Ground, MD (TEDT-AT-WFT (F. Carlen))	1
U.S. Army Natick Soldier Research, Development, and Engineering Center, Natick, MA (R. Benney, P. Blanas, P. Cunniff, K. Horak, M. Jee, J. Mackiewicz, M. Maffeo, G. Proulx, C. Quigley, R. Sykes, G. Thibault, S. Tucker, J. Ward)	13
U.S. Army Research Office (RDRL-RO-EN (D. Stepp, W. Mullins))	2
Navy Clothing and Textile Research Facility, Natick, MA (B. Avellini, L. Caulfield, T. Hart, C. Heath)	4
Naval Surface Warfare Center, Panama City, FL (Code CX05 (F. Garcia))	1
Naval Surface Warfare Center, Carderock Division, W. Bethesda, MD (P. Dudt, R. Crane, E. Rasmussen)	3
Naval Surface Warfare Center, Dahlgren Division, Dahlgren, VA (S. Bartyczak, W. Mock)	2
Office of Naval Research, Arlington, VA (ONR-331 (R. Barsoum), ONR-DOI (L. Schuette), ONR-334 (Y. Rajapakse))	3
Defense Technical Information Center	1
Center for Naval Analyses	1
University of Rhode Island, Kingston, RI (A. Shukla)	1
City College of the City University of New York, NY (A. Sadegh)	1
University of British Columbia, Kelowna, BC, Canada (A. Milani)	1
JPS Composite Materials, Anderson SC (M. Salama)	1
Core Composites, Bristol, RI (R. O'Meara)	1
Warwick Mills, New Ipswich, NH (C. Howland)	1